AFRL-OSR-VA-TR-2013-0133

A New Multiscale Methodology for Evaluating Distributions of Residual Stress in Processed Aerospace Alloys

Matthew Miller, Paul Dawson, James Williams and Jun-Sang Park

Cornell University

March 2013
Final Report

DISTRIBUTION A: Approved for public release.

AIR FORCE RESEARCH LABORATORY
AF OFFICE OF SCIENTIFIC RESEARCH (AFOSR)
ARLINGTON, VIRGINIA 22203
AIR FORCE MATERIEL COMMAND

REPORT DOCUMENTATION PAGE

Form Approved
OMB No. 0704-0188

The public reporting burden for this collection of information is estimated to average 1 hour per response, including the time for reviewing instructions, searching existing data sources, gathering and maintaining the data needed, and completing and reviewing the collection of information. Send comments regarding this burden estimate or any other aspect of this collection of information, including suggestions for reducing the burden, to the Department of Defense, Executive Services and Communications Directorate (0704-0188). Respondents should be aware that notwithstanding any other provision of law, no person shall be subject to any penalty for failing to comply with a collection of information if it does not display a currently valid OMB control number.

PLEASE DO NOT RETURN YOUR FORM TO THE ABOVE ORGANIZATION.

1. REPORT DATE *(DD-MM-YYYY)*	2. REPORT TYPE	3. DATES COVERED *(From - To)*
13-02-2013	FNAL	09012009-08312012

4. TITLE AND SUBTITLE

A New Multiscale Methodology for Evaluating Distributions of Residual Stress in Processed Aerospace Alloys

5a. CONTRACT NUMBER

5b. GRANT NUMBER

FA9550-09-1-0642

5c. PROGRAM ELEMENT NUMBER

6. AUTHOR(S)

Miller, Matthew, P., Dawson, Paul, R. Williams, James, C. and Park, Jun-Sang

5d. PROJECT NUMBER

5e. TASK NUMBER

5f. WORK UNIT NUMBER

7. PERFORMING ORGANIZATION NAME(S) AND ADDRESS(ES)

Cornell University
373 Pine Tree Rd. Ithaca,NY 14850

8. PERFORMING ORGANIZATION REPORT NUMBER

9. SPONSORING/MONITORING AGENCY NAME(S) AND ADDRESS(ES)

AFOSR
875 N Randolph St
Arlington, VA 22203

10. SPONSOR/MONITOR'S ACRONYM(S)

11. SPONSOR/MONITOR'S REPORT NUMBER(S)

AFRL-OSR-VA-TR-2013-0133

12. DISTRIBUTION/AVAILABILITY STATEMENT

DISTRIBUTION A: APPROVED FOR PUBLIC RELEASE

13. SUPPLEMENTARY NOTES

14. ABSTRACT

This project focused on the development of a new method for determining residual stress fields in poly- crystalline metallic alloys using high energy synchrotron x-ray diffraction measurements and a finite element discretization of the workpiece. At each diffraction volume, the diffraction data provides a link to the single grain scale stresses through pole figures of lattice strain. An optimization method produces the macroscale residual stress for every point in the body that satisfies equilibrium on the macroscale and is simultaneously consistent with the grain scale stress at the diffraction volumes. The method was demonstrated on four different test scenarios: (i) conventional nickel shrink-fit disk (producing a 2D stress field), (ii) a tapered nickel shrink fit disk (producing a 3D stress field), (iii) a titanium shrink fit disk (demonstration with hcp material and (iv) a shot peened sample (demonstration on an important appli- cation. All experiments were conducted at the Advanced Photon Source. The synchrotron radiation and high-throughput area detectors were ideal for proving up the new method.

15. SUBJECT TERMS

16. SECURITY CLASSIFICATION OF:			17. LIMITATION OF ABSTRACT	18. NUMBER OF PAGES	19a. NAME OF RESPONSIBLE PERSON
a. REPORT	b. ABSTRACT	c. THIS PAGE			Matthew P. Miller
U	U	U	U	15	19b. TELEPHONE NUMBER *(Include area code)* 607.255.0400

Reset

Standard Form 298 (Rev. 8/98)
Prescribed by ANSI Std. Z39.18

INSTRUCTIONS FOR COMPLETING SF 298

1. REPORT DATE. Full publication date, including day, month, if available. Must cite at least the year and be Year 2000 compliant, e.g. 30-06-1998; xx-06-1998; xx-xx-1998.

2. REPORT TYPE. State the type of report, such as final, technical, interim, memorandum, master's thesis, progress, quarterly, research, special, group study, etc.

3. DATES COVERED. Indicate the time during which the work was performed and the report was written, e.g., Jun 1997 - Jun 1998; 1-10 Jun 1996; May - Nov 1998; Nov 1998.

4. TITLE. Enter title and subtitle with volume number and part number, if applicable. On classified documents, enter the title classification in parentheses.

5a. CONTRACT NUMBER. Enter all contract numbers as they appear in the report, e.g. F33615-86-C-5169.

5b. GRANT NUMBER. Enter all grant numbers as they appear in the report, e.g. AFOSR-82-1234.

5c. PROGRAM ELEMENT NUMBER. Enter all program element numbers as they appear in the report, e.g. 61101A.

5d. PROJECT NUMBER. Enter all project numbers as they appear in the report, e.g. 1F665702D1257; ILIR.

5e. TASK NUMBER. Enter all task numbers as they appear in the report, e.g. 05; RF0330201; T4112.

5f. WORK UNIT NUMBER. Enter all work unit numbers as they appear in the report, e.g. 001; AFAPL30480105.

6. AUTHOR(S). Enter name(s) of person(s) responsible for writing the report, performing the research, or credited with the content of the report. The form of entry is the last name, first name, middle initial, and additional qualifiers separated by commas, e.g. Smith, Richard, J, Jr.

7. PERFORMING ORGANIZATION NAME(S) AND ADDRESS(ES). Self-explanatory.

8. PERFORMING ORGANIZATION REPORT NUMBER. Enter all unique alphanumeric report numbers assigned by the performing organization, e.g. BRL-1234; AFWL-TR-85-4017-Vol-21-PT-2.

9. SPONSORING/MONITORING AGENCY NAME(S) AND ADDRESS(ES). Enter the name and address of the organization(s) financially responsible for and monitoring the work.

10. SPONSOR/MONITOR'S ACRONYM(S). Enter, if available, e.g. BRL, ARDEC, NADC.

11. SPONSOR/MONITOR'S REPORT NUMBER(S). Enter report number as assigned by the sponsoring/ monitoring agency, if available, e.g. BRL-TR-829; -215.

12. DISTRIBUTION/AVAILABILITY STATEMENT. Use agency-mandated availability statements to indicate the public availability or distribution limitations of the report. If additional limitations/ restrictions or special markings are indicated, follow agency authorization procedures, e.g. RD/FRD, PROPIN, ITAR, etc. Include copyright information.

13. SUPPLEMENTARY NOTES. Enter information not included elsewhere such as: prepared in cooperation with; translation of; report supersedes; old edition number, etc.

14. ABSTRACT. A brief (approximately 200 words) factual summary of the most significant information.

15. SUBJECT TERMS. Key words or phrases identifying major concepts in the report.

16. SECURITY CLASSIFICATION. Enter security classification in accordance with security classification regulations, e.g. U, C, S, etc. If this form contains classified information, stamp classification level on the top and bottom of this page.

17. LIMITATION OF ABSTRACT. This block must be completed to assign a distribution limitation to the abstract. Enter UU (Unclassified Unlimited) or SAR (Same as Report). An entry in this block is necessary if the abstract is to be limited.

A New Multiscale Methodology for Evaluating Distributions of Residual Stress in Processed Aerospace Alloys

Research funded under the AFOSR Multi-Scale Structural Mechanics Program

FA9550-09-1-0642

Dr. David Stargel, Program Manager

Final Report

Paul Dawson[1], Matthew Miller[1], Kevin McNelis[1], Amanda Oczkowski[1], Jun-Sang Park[1] and James Williams[2]

[1]Sibley School of Mechanical and Aerospace Engineering
Cornell University, Ithaca NY 14853

[2]Department of Materials Science and Engineering
The Ohio State University, Columbus Ohio 43210

Abstract

This project focused on the development of a new method for determining residual stress **fields** in polycrystalline metallic alloys using high energy synchrotron x-ray diffraction measurements and a finite element discretization of the workpiece. At each diffraction volume, the diffraction data provides a link to the single grain scale stresses through pole figures of lattice strain. An optimization method produces the macroscale residual stress for every point in the body that satisfies equilibrium on the macroscale and is simultaneously consistent with the grain scale stress at the diffraction volumes. The method was demonstrated on four different test scenarios: (i) conventional nickel shrink-fit disk (producing a 2D stress field), (ii) a tapered nickel shrink fit disk (producing a 3D stress field), (iii) a titanium shrink fit disk (demonstration with hcp material and (iv) a shot peened sample (demonstration on an important application. All experiments were conducted at the Advanced Photon Source. The synchrotron radiation and high-throughput area detectors were ideal for proving up the new method. This final report described the four application and summarizes the project

1 Method Overview

Figure 1 depicts an overview schematic of the approach we have employed for measuring lattice strains and determined residual stress distributions within an engineering component. The upper left corner shows a shrink fit disk whose stress field varies over the disk. As can be seen, the radial and circumferential normal stresses can be approximated using a closed form solution based on the magnitude of the interference and the material property of the disk. However, the determination of the actual stress field in the disk remains a challenging problem.

The methodology we have developed quantifies the residual stress tensor field over a component by coupling lattice strains measured using high-energy, synchrotron x-ray diffraction with a solution framework that simultaneously determines the stress distribution over all crystal orientations AND the macroscopic stress distribution. The technique is a non-destructive diffraction method. However, it differs from many current non-destructive measures of residual stress by utilizing a large number of lattice strain measurements that are not limited to the surface (or near surface) of a part. Synchrotron x-rays and high speed detectors enable making thousands of lattice strain measurements within a body in reasonable experimental times. The challenge as it relates to residual stress analyses is how to use this abundance

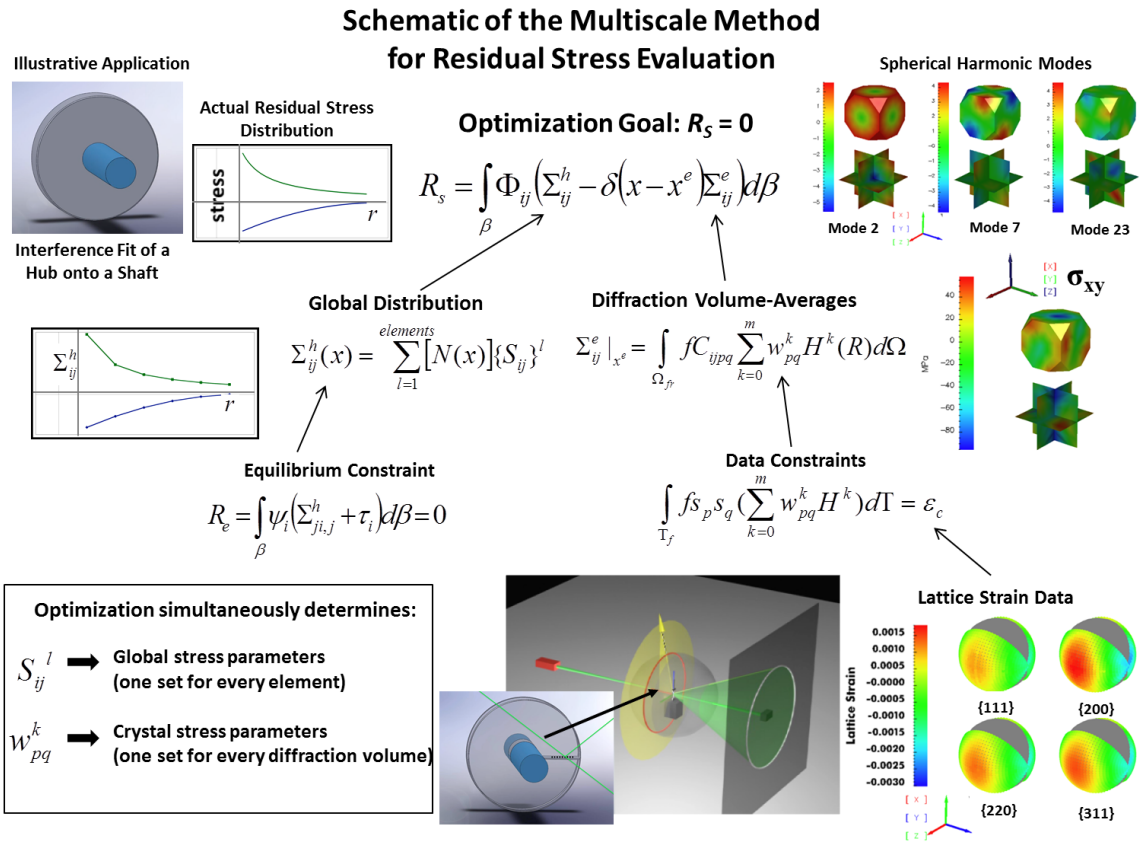

Figure 1: Schematic of the multiscale method for determining the residual stress in engineering components. The method considers the material response at both the macro- and micro-scales. The method is set up as an objective function with explicit constraints, relating the macroscopic stress distribution to the diffraction volume average crystal stress.

of measurements to fully characterize the state of stress within an engineering component.

Rather than interpreting the lattice strain data obtained as a particular material point (or a diffraction volume) as simple strain gauge measurements and using isotropic material property to determine the components of residual stresses in an engineering component, we start with the assumption that the average of the crystal scale stresses properly integrated over an aggregate of crystals should coincide with the stress in the contiuum scale at a particular material point. With this in mind, we interpret the lattice strain data as a crystallographic fiber average quantity described as

$$\epsilon_{\boldsymbol{qq}} = \frac{\int_{\Upsilon_{\boldsymbol{c}\|\boldsymbol{q}}} \mathcal{A}(\boldsymbol{r})\boldsymbol{q}\cdot\boldsymbol{\epsilon}(\boldsymbol{r})\cdot\boldsymbol{q}d\boldsymbol{r}}{\int_{\Upsilon_{\boldsymbol{c}\|\boldsymbol{q}}} \mathcal{A}(\boldsymbol{r})d\boldsymbol{r}} \tag{1}$$

.

In this equation, $\epsilon_{\boldsymbol{qq}}$ is the lattice strain measured along a particular scattering direction, $\boldsymbol{q}$, for a particular family of family of crystallogprahic plane, $\boldsymbol{c}$, $\mathcal{A}(\boldsymbol{r})$ is the crystallographic orientation distribution function of the diffraction volume and $\boldsymbol{\epsilon}(\boldsymbol{r})$ is the lattice strain distribution function (LSDF) - an orientation dependent elastic strain tensor.

Using appropriate anisotropic elasticity, Equation 1 can be rewritten as

$$\epsilon_{\boldsymbol{qq}} = \frac{\int\limits_{\Upsilon_{\boldsymbol{c}\|\boldsymbol{q}}} \mathcal{A}(\boldsymbol{r})\boldsymbol{q}\cdot\boldsymbol{S}(\boldsymbol{r})\boldsymbol{\sigma}(\boldsymbol{r})\cdot\boldsymbol{q}d\boldsymbol{r}}{\int\limits_{\Upsilon_{\boldsymbol{c}\|\boldsymbol{q}}} \mathcal{A}(\boldsymbol{r})d\boldsymbol{r}} \tag{2}$$

where $\boldsymbol{S}(\boldsymbol{r})$ is the anisotropic single crystal compliance and $\boldsymbol{\sigma}(\boldsymbol{r})$ is the orientation dependent crystal stresses or the stress orientation distribution function (SODF).

Using the SODF and the orientation distribution function of the diffraction volume, the stress at the continuum scale is obtained by

$$\boldsymbol{\Sigma}^e = \frac{\int\limits_{\Omega_{\text{fr}}} \mathcal{A}(\boldsymbol{r})\boldsymbol{\sigma}(\boldsymbol{r})d\boldsymbol{r}}{\int\limits_{\Omega_{\text{fr}}} \mathcal{A}(\boldsymbol{r})d\boldsymbol{r}} \tag{3}$$

where $\boldsymbol{\Sigma}^e$ is the stress at the continuum scale and Ω_{fr} is the fundamental region of orientation space for a particular crystal symmetry.

A common method for representing and computing a field over the crystallographic orientation space is to use a piecewise interpolation functions over the crstallogrpahic orientation space [1]. However, this can be costly when many diffraction volumes are considered simultaneously. Instead, we use a set of orthonormal functions defined over orientation space[1] and corresponding coefficients. For example, a component of $\boldsymbol{\sigma}(\boldsymbol{r})$ at a particular diffraction volume, denoted as $\sigma_{pq}(\boldsymbol{r})$, is represented as

$$\sigma_{pq}(\boldsymbol{r}) = \sum_{m=1}^{m_{max}} H^m(\boldsymbol{r}) w_{pq}^m \tag{4}$$

where $\sigma_{pq}(\boldsymbol{r})$ is the pq component of $\boldsymbol{\sigma}(\boldsymbol{r})$, $H^m(\boldsymbol{r})$ is the mth orthnomal function defined over orientation space, w_{pq}^m is the corresponding coefficient, and m_{max} is the maximum number of orthonomal functions considered.

Interrogating many diffraction volumes over the engineering component allows us to obtain $\boldsymbol{\Sigma}^e$ at those diffraction volumes. However, $\boldsymbol{\Sigma}^e$ does not necessarily satisfy the boundary conditions of the engineering component or equilibirum. To utilize these pieces of information from the the continuum scale and $\boldsymbol{\Sigma}^e$ information obtained from the crystal length scale, piecewise interpolation functions over the physical body of the engineering component are used to determine the residual stress field ($\boldsymbol{\Sigma}^h$). This field not only satisfies the boundary conditions and equilibrium at the continuum scale but also matches $\boldsymbol{\Sigma}^e$ where diffraction measurements are made[2].

In our first benchmarking effort to explore the capability of this new method, we determined the distribution of stresses over an interference fit, hub-shaft assembly. There is a well-known analytic approximation of the circumferential and radial normal stresses. This sample, which was described in the year 1 progress report, is one that has been used in previous residual stress analyses as a benchmarking example. We measure lattice strain pole figures at a span of points over the component. As depicted in Figure 1, the overall goal of our methodology is to then minimize a residual, R_s, that has been defined over the part, which equates the macroscopic stress distribution to the volume averaged crystal stress at a discrete number of the diffraction measurement locations. The resulting stress distributions over every

[1] These functions are known as spherical harmonic functions in quantitative texture analysis.

[2] The readers are referred to McNelis et al [2] and Demir et al [3] for a more detailed presentation of the method.

aggregate within the component and over every orientation within each aggregate are constructed to best match the strain pole figure data while satisfying stress equilibrium at the macroscale and the stress boundary conditions of the specimen. Our formulation consists of finite element discretizations of both the component itself and the space of all crystal orientations within an individual aggregate. Figure 1 depicts graphically the development of the macro- and micro-stress expressions.

The stress at the crystal scale is first established by making diffraction measurements at discrete points over a quadrant of the sample. These diffraction measurements provide the projection of the crystal lattice strain in many directions, and serve as an experimental constraint: any stress solution must produce lattice strains in agreement with what is measured experimentally. Several Strain Pole Figures (SPFs), which plot the projection of the strain tensor for certain lattice planes aligned with different sample directions, are shown at the bottom-right of Figure 1. These experimental measurements serve as the driving force for the solution method. Using these lattice strains, we can quantify the average stress tensor as a function of crystal orientation in each diffraction volume. The process for doing so proceeds up the right hand side of Figure 1. We choose to represent the orientation dependent crystal stresses in each diffraction volume through a spherical harmonic expansion over orientation space. Several harmonic modes (evaluated over orientation space) are provided in the upper-right of Figure 1, as well as an example of one component of the crystal stress tensor for a diffraction volume. The set of unknowns for the description of the crystal scale response are the coefficients in the harmonic expansion for each diffraction volume We can integrate over orientation space in order to determine the crystal-averaged stress tensor for each diffraction volume. These values define one half of the expression for the global residual.

These crystal averaged stresses are then related to the macroscopic stress through a novel solution framework. The framework for the macroscopic description is provided along the left hand side of Figure 1. The analytic solution for the principal stress components in the hub of the interference fit assembly is given in the upper-left corner. It is this distribution that we are attempting to solve for using our multiscale approach. As can be seen, the radial and circumferential stress vary with radial position. The actual distribution may vary from this idealization. We first discretize the component using finite elements, and represent the macroscopic stress distribution over the body as the mapping of the stress tensor at discrete nodal points using finite element shape functions. We constrain the solution for the macroscopic stress tensor field such that it is self-equilibrating over the body. The value of the macroscopic stress tensor at these nodal points, S_{ij}^{l}, serve as the second set of unknowns in the problem statement. As described in year 2 progress report, we have developed a moving least squares (MLS) formulation to decouple the spatial relationship between the physical diffraction volume and the finite element mesh of the part. In our year 1, the finite element mesh of the part was generated such that the centroid of a finite element coincided with the location on the part where diffraction measurement took place. However, it may be impossible to lay out a regular grid of measurement over a part. By introducing the MLS formulation, the centroid of a finite element does not have to coincide with the location on the part where the lattice strains are measured; this allows the multiscale optimization to deal with irregularly shaped parts and use lattice strain measurements from irregularly located diffraction volumes.

The optimization is set up to simultaneously determine both the values of the macroscopic stress tensor at the nodal points of the discretized part, as well as the series of spherical harmonic coefficients describing the orientation dependent crystal stress in each diffraction volume. The method is unique in that it contains information regrading both the micro- and macro-scale response of the component. In residual stress analysis, stresses at different size scales are often referred to as 'types' of residual stress. Type I residual stress refers to a stress averaged over a volume containing many grains (usually several thousand). Type II residual stress considers stress as a function of each crystal in the aggregate. In the method we have outlined, the macroscopic residual stress at the nodal points of the part is a type I residual stress. Meanwhile, the spherical harmonic coefficients that define the crystal stress in each diffraction volume is similar in nature to type II residual stress. They differ somewhat in that the crystal stress is averaged for all grains in that diffraction volume which have a common crystallographic

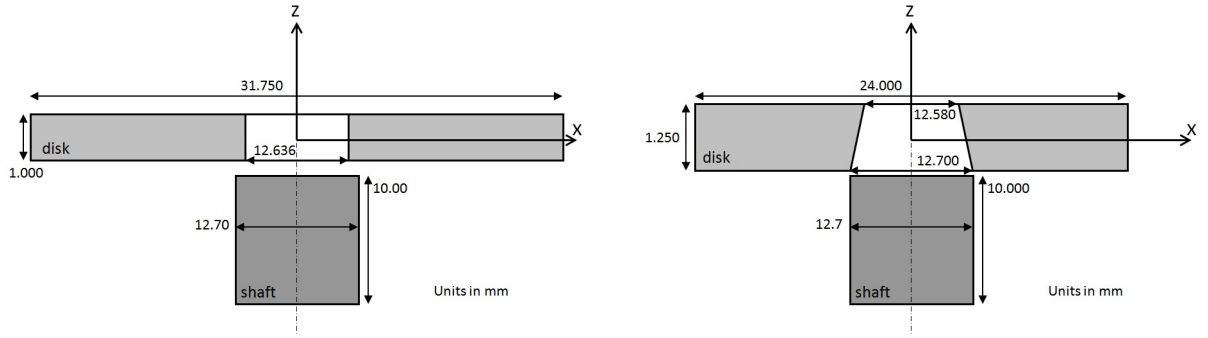

(a) Sample geometry A. In this geometry, the center hole of the hub is not tapered and the ideal stress field in the hub is expected to be constant through the thickness and only expected to vary in the x-y plane.

(b) Sample geometry B. In this geometry, the center hole of the hub is tapered and the anticipated stress field in the hub is expected to vary both in the x-y plane and through the thickness.

Figure 2: Two shrink fit sample geometries considered in this work.

orientation.

In this project, we have developed a method for determining the 3D residual stress fields in polycrystalline components using high energy x-ray diffraction together with a finite element-based multiscale optimization methodology. The two important aspects of the formulation are: (i) experiments to measure lattice Strain Pole Figures (SPFs) at multiple points throughout an engineering component using synchrotron x-ray diffraction and (ii) a finite element based method for determining the stress distributions that best match the SPF data and are consistent with conditions such as stress equilibrium and boundary conditions at the macroscale. A residual-based optimization formulated to determine the "best" macroscopic stress distribution consistent with both the lattice strain measurements and the constraint conditions from the macroscale.

2 Accomplishments

Two shrink-fit geometries were used (Figure 2) to develop and validate the methodology. The hub in these geometries were manufactured from LSHR (Low Solvus High Refractory) nickel base alloy. For sample geometry A, we were able to measure many SPFs for material points located throughout the sample in the x-y plane using the SPF measurement technique [4, 2]. In this case, the stresses through the thickness of the hub were expected to be constant and the material points through the thickness of the hub at a particular (x,y) position were not distinguished. On the other hand, for sample geometry B, we measured the SPFs for a material point located at a particular (x,y,z) by modifying the SPF measurement technique and isolating a particular material point in thin the hub. Using these SPF measurements and the multiscale optimization method, we were able to determine the 3D residual stress fields in sample A and B non-destructively.

To test the new methodology, we attempted to quantify the residual stress field in a titanium component. In this case, the hub in sample geometry A was manufactured from Titanium Ti-8Al-1Mo-1V (Ti-811) alloy. A set of SPFs were measured in the hub. The SPF data were used to determine the residual stress field in the hub employing our multiscale optimization. The SPF data were also used to determine the residual stresses employing the conventional $\sin^2 \Psi$ method at the material points where the SPF data were obtained. The stresses these two approaches were compared.

We also attempted to expand the methodology to an industrial application. A LSHR tension sample was shot-peened and the lattice strains at the material points located inside the sample were measured. These strains were used in conjunction with the multiscale optimization method to determine the residual

stress field introduced by the shot-peening process. These residual stresses were compared to the residual stresses quantified by laboratory x-ray systems and the $\sin^2 \Psi$ method.

3 Residual Stress in sample geometry A

The interference fit disk geometry particularly attractive for testing our methodology as a closed form solution of the stress distribution in the hub exists. Figure 3 shows the comparison between the closed form stress results and the stresses from out multiscale optimization method. Trends in the data should compare to the closed form results. As can be seen, the stresses from the multiscale optimization method that uses the strain pole figure measurements contain real artifacts that render the distributions less "perfect" than the closed form solution. However, the trends from the analytic solution can be seen in data. The absolute values are not exact matches but the comparison of the trends is extremely encouraging. The residual stress field in this sample was also evaluated using the multiscale optimization method with the moving least square formulation. As can be seen, the resulting stress distributions contain the same general stress information as the constant stress element results shown in Figure 3 but appear to have smoother, more physically realizable transition regions. We feel that the resulting stress solution using the MLS method will produce greater accuracy and, more importantly, will decouple the diffraction measurements from the underlying finite element mesh.

A paper describing the 2D results on the LSHR specimen was submitted to the Journal of Mechanics and Physics of Solids and is in press [2]. A paper describing the multiscale optimization with moving least squares formulation was submitted to Computer Methods in Applied Mechanics and Engineering [3].

4 Residual Stress in sample geometry B

Residual stress fields are not necessarily two dimensional. The next thrust in the project was focused on creating the ability to measure lattice strain pole figures over an object with its stress field varying in all three dimensions in a non-destructive manner and using these strain pole figure measurements with the multiscale optimization method to determine the stress field in the object. For this objective, a sample employing geometry B was manufactured.

Making subsurface lattice strain measurements presents a distinct experimental challenge. We made use of the conical slit setup at APS 1-ID-C to measure the strain pole figures for many internal diffraction volumes. Figure 4 shows a subset of SPFs obtained by the conical slit setup. In this figure, the radial position on the hub, r_S, is measured on the x-y plane of the sample and the azimuthal angle on the hub, α_S, is measured from the x-axis of the sample. When the interference is large, the magnitude of lattice strains are large. If the interference is small, the magnitude of lattice strains are small. Also, the lattice strains are larger at the inner radial position than those at the outer radial position. In total, 196 diffraction volumes located throughout the hub were interrogated and {111}, {200}, and {220} strain pole figures were measured at each diffraction volume. It is also worthwhile to note that the highs and the lows in the SPFs measured at $\alpha_S = 0^\circ$ and the highs and the lows in the SPFs measured at $\alpha_S = 90^\circ$ are $\alpha_S = 90^\circ$ apart. This is consistent with the anticipated state of stress in this sample.

Using these strain pole figures and the multiscale optimization method with moving least squares formulation, the residual stress field in sample B were determined. Figure 5 shows the analytical interference fit stress and the residual stress field obtained by using the strain pole figure measurements shown in Figure 4 and the multiscale optimization method with moving least squares formulation. The results are encouraging. The highs and the lows in the residual stress distribution are consistent with the interference introduced by the sample geometry. This work was submitted to Experimental Mechanics [5].

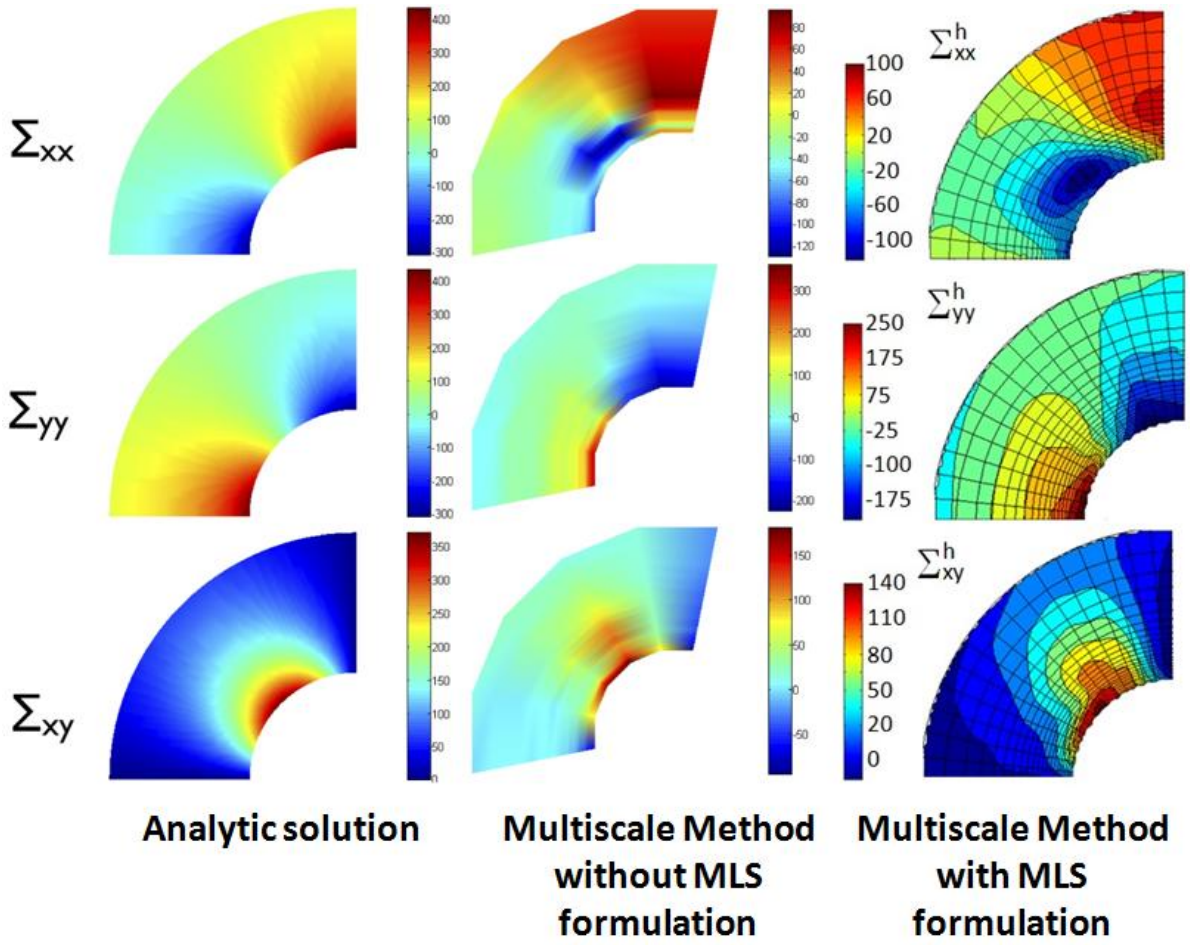

Figure 3: Analytic shrink fit approximation (left) and residual stress distributions determined using the strain pole figure measurements and our new formulation without the moving least squares formulation (center) and with the moving least squares formulation (right).

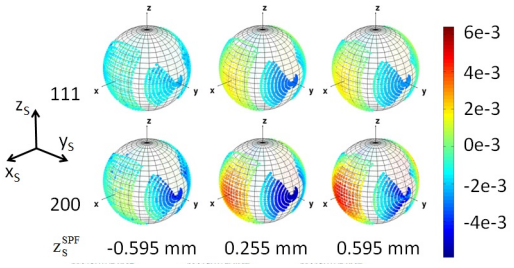

(a) The SPFs for {111} and {200} from several internal positions at $r_S = 6.85$ mm and $\alpha_S = 0°$.

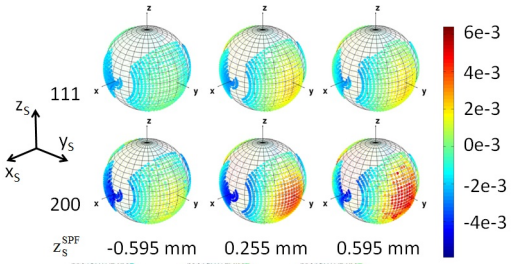

(b) The SPFs for {111} and {200} from several internal positions at $r_S = 6.85$ mm and $\alpha_S = 90°$.

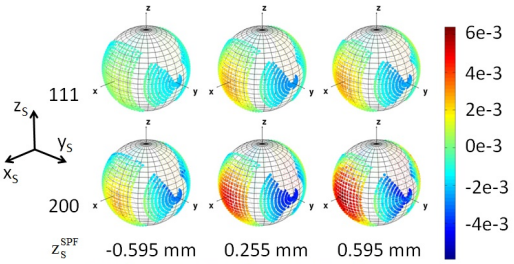

(c) The SPFs for {111} and {200} from several internal positions at $r_S = 7.80$ mm and $\alpha_S = 0°$.

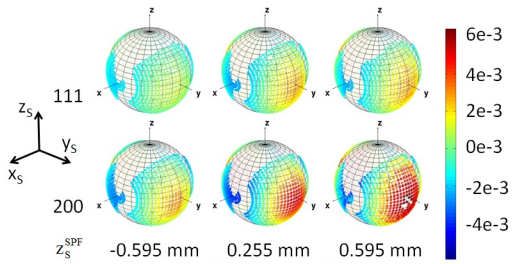

(d) The SPFs for {111} and {200} from several internal positions at $r_S = 7.80$ mm and $\alpha_S = 90°$.

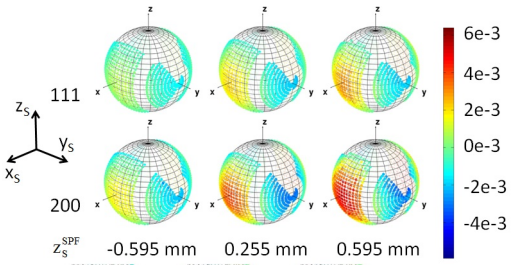

(e) The SPFs for {111} and {200} from several internal positions at $r_S = 9.30$ mm and $\alpha_S = 0°$.

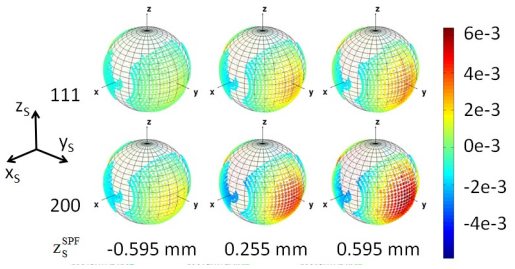

(f) The SPFs for {111} and {200} from several internal positions at $r_S = 9.30$ mm and $\alpha_S = 90°$.

Figure 4: A subset of SPFs measured using the conical slit setup for sample geometry B. Figures 4(a), 4(a), and 4(e) show a set of SPFs from three r_S positions along $\alpha_S = 0°$. Figures 4(b), 4(d) and 4(f) show a set of SPFs from three r_S positions along $\alpha_S = 90°$.

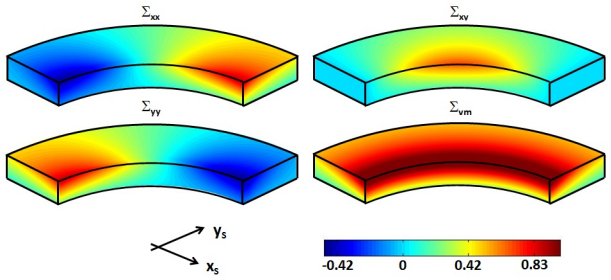

(a) An approximation of the stress field in the interference fit sample obtained by a 3D elastic FE simulation of a quarter of the disk. The stress field is normalized by the maximum of the second invariant of the stress to show the anticipated trends of the stress field. Two normal components and one shear component of the stress, denoted by Σ_{xx}, Σ_{yy}, and Σ_{xy} respectively, are shown. The values of the other stress components are negligible. The second invariant stress denoted by Σ_{vm} is also shown.

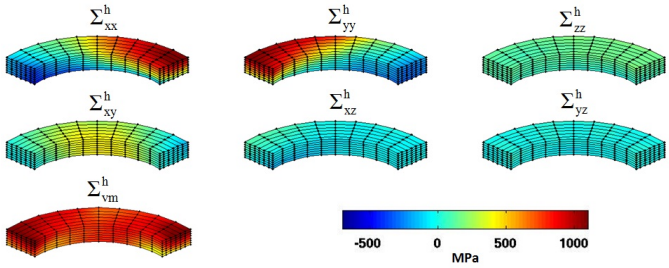

(b) The components of the 3D residual stress field and the von Mises effective stress of the disk obtained by combining the SPF data and the bi-scale optimization scheme are plotted over the FE mesh of the disk. The coordinate system is the same as that in Figure 5(a).

Figure 5: Analytical interference fit stress for sample geometry B and and the stress field obtained by using the strain pole figure measurements shown in Figure 4.

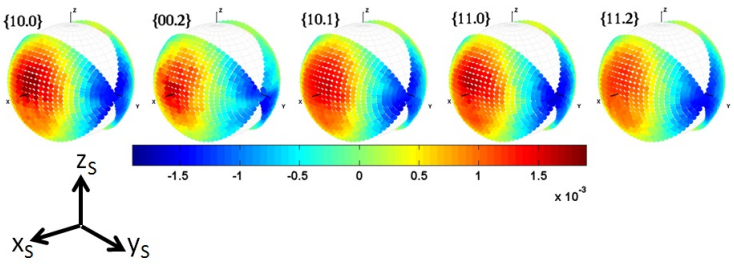

(a) The SPFs from inner most positions on the hub at $\alpha_S = 0°$.

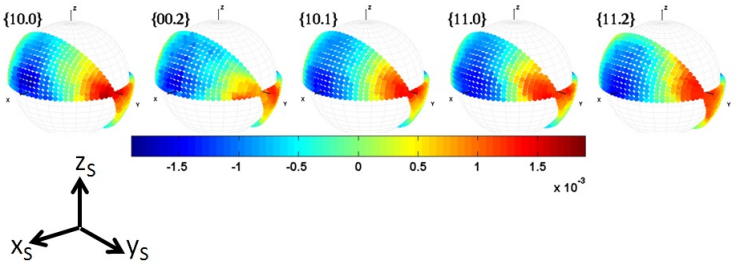

(b) The SPFs from inner most positions on the hub at $\alpha_S = 90°$.

Figure 6: A subset of SPFs measured for the Ti-811 interference fit sample.

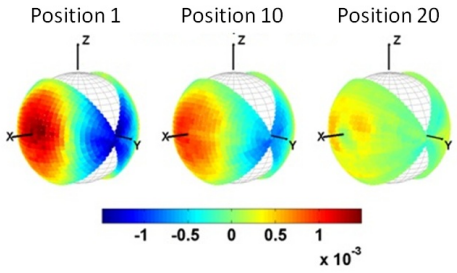

Figure 7: The {10.1} SPFs from at $\alpha_S = 0°$ measured at several radial positions. Position 1 is the innermost radial position and Position 20 is the outermost radial position.

5 Residual Stress in the Ti-811 sample

A titanium sample was manufactured using geometry A. The hub was made from a Ti-811 alloy. Similar to the LSHR samples, strain pole figures were measured at several locations throughout the hub. Figures 6 and 7 show a subset of the strain pole figures measured for the Ti-811 sample. Similar to the LSHR samples, the lattice strains are consistent with the anticipated stress distribution of the interference fit geometry.

These strain pole figure data are used to determine the residual stress field in the hub. Figure 8 shows the result. Again, the residual stress field determined from the experimental data and the multiscale optimization method is similar to the anticipated stress in an interference fit geometry. However, unlike the analytical solution where the Σ^h_{xx} and Σ^h_{yy} are mirror images of each other, the two components in the residual stress field that we have determined from the SPF measurements show differences. This is expected as obtaining a perfect interference around the azimuth of the hub (which is assumed in the analytic solution for interference fit geometry) is difficult.

We also used the SPF measurements with the conventional $\sin^2\Psi$ method to determine the stresses at several locations on the hub and compared these stresses with the 3D residual stress field that we obtained using the multiscale optimization method. Using lattice strain data from {11.2} SPFs and appropriate

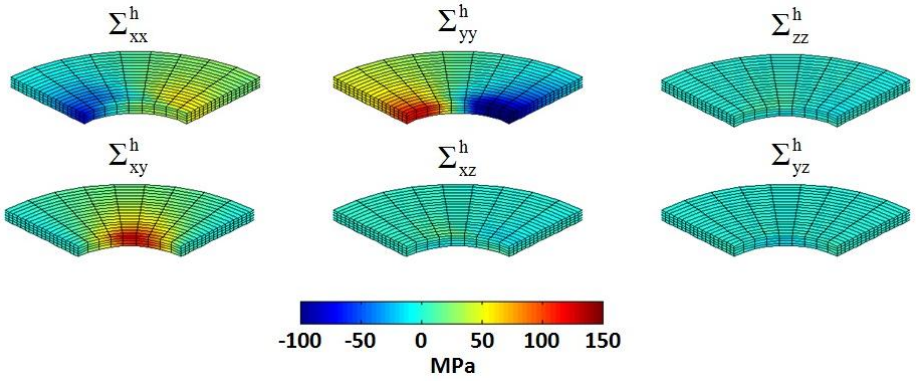

Figure 8: The components of the 3D residual stress field determined from the strain pole figures and the multiscale optimization method. The coordinate system is the same as that in Figure 5(a).

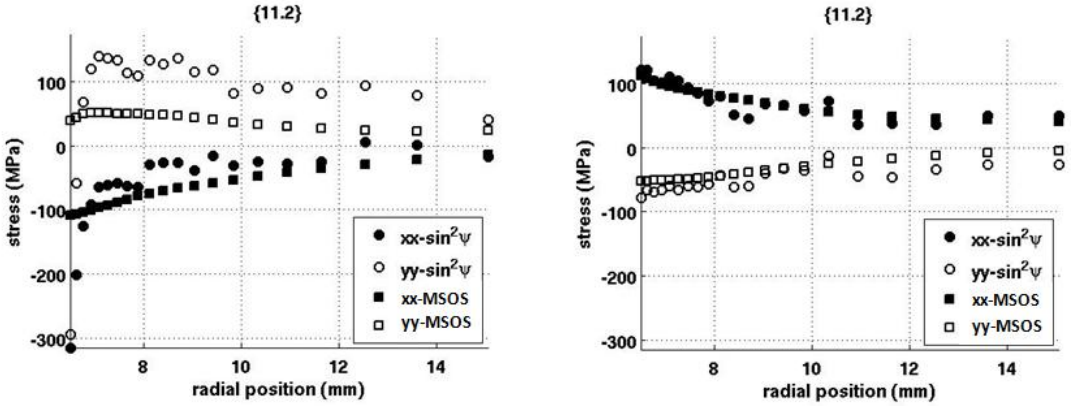

(a) The xx- and yy- components of residual stress at $\alpha_S = 0^\circ$ obtained by the $\sin^2\Psi$ analysis using {11.2} reflection and multiscale optimization stresses using the full strain pole figure data.

(b) The xx- and yy- components of residual stress at $\alpha_S = 90^\circ$ obtained by the $\sin^2\Psi$ analysis using {11.2} reflection and the multiscale optimization stresses using the full strain pole figure data.

Figure 9: A comparison of xx- and yy- components of stresses obtained by the $\sin^2\Psi$ analysis and the multiscale optimization method.

material properties for the $\sin^2\Psi$, the xx- and the yy- components of stresses were found and were compared to the those obtained by the multiscale optimization method. Figure 9 shows the comparison between the two methods at $\alpha_S = 0^\circ$ and $\alpha_S = 90^\circ$. This figure shows that the stresses obtained by the two methods can be significantly different (Figure 9(a)) or comparable (Figure 9(b)). Because the $\sin^2\Psi$ does not compute the entire stress field and does not make use the macroscopic constraints such as equilibrium while over simplifying the nature of the lattice strain measurements, we think that the residual stress field obtained by the multiscale optimization method is more reliable. A journal manuscript for this work on the titanium sample is in preparation.

6 Residual Stress field in a shot-peened sample

In collaboration with researchers at Wright Patterson AFB - Materials Directorate, a set of conical slit experiments were performed on an Inconel 100 sample that has been subjected to shot peening. Figure 10 shows the geometry of the sample and lists the locations in the sample where x-ray diffraction experiments

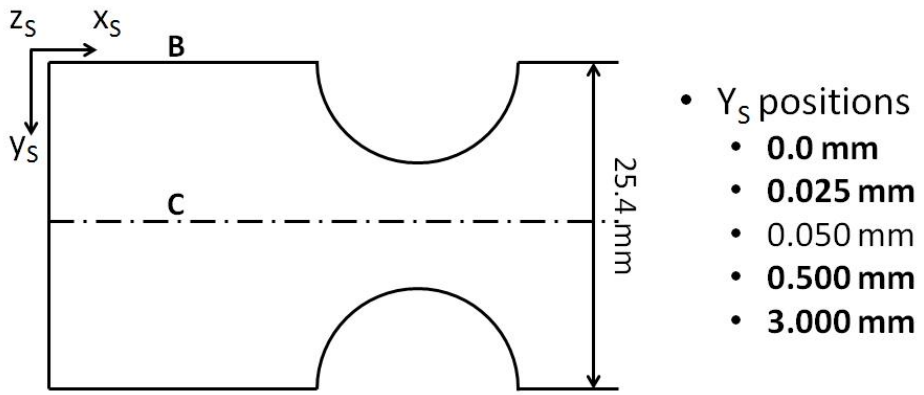

Figure 10: A schematic of the shot peened sample. The thickness through z_S is 2 mm.

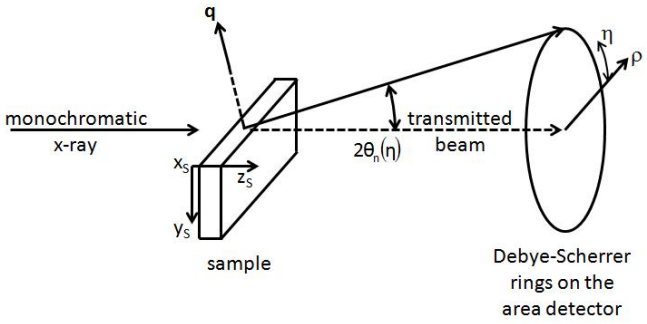

Figure 11: A schematic of the experimental geometry used to investigate the shot peened sample.

using the conical slit setup were performed. All surfaces of the sample were shot peened. Here, we assume that the shot peened produces a stress distribution that is independent of x_S. Figure 11 shows the experimental geometry used to investigate the shot peened sample.

Figure 12 shows the lattice strains measured in normal incidence (z_S parallel to the incident beam path) at various y_S positions for three crystallographic planes. Here, the stress in the shot peened sample is assumed to be independent of x_S and the location of the diffraction volumes only depends on y_S and z_S. This figure shows that the magnitudes of lattice strains from the shot peening process are large near the surface and are smaller in the interior. By $y_S = 0.500$mm, the lattice strains are close to zero for all three crystallographic planes.

While this does not cover the entire strain pole figure surface, a 3D residual stress field for the shot

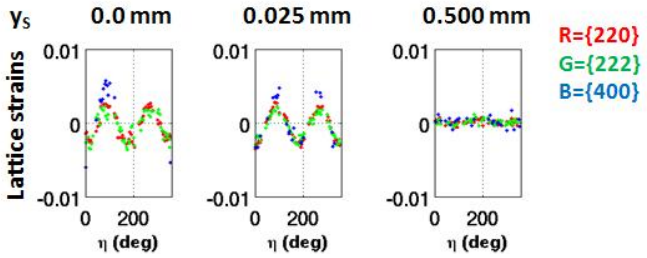

Figure 12: A subset of the lattice strains measured in normal incidence (z_S parallel to the incident beam path) at various y_S positions for three crystallographic planes.

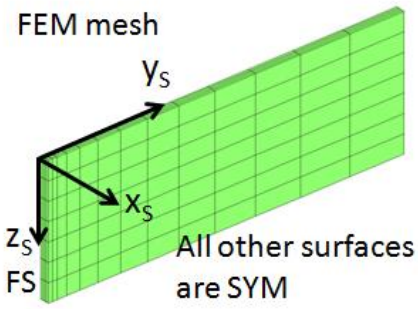

Figure 13: The finite element mesh used to perform the multiscale optmization method with the lattice strain data. The x_S-z_S surface is a free surface and all other surfaces are symmetric surfaces where the in-plane tractions vanish.

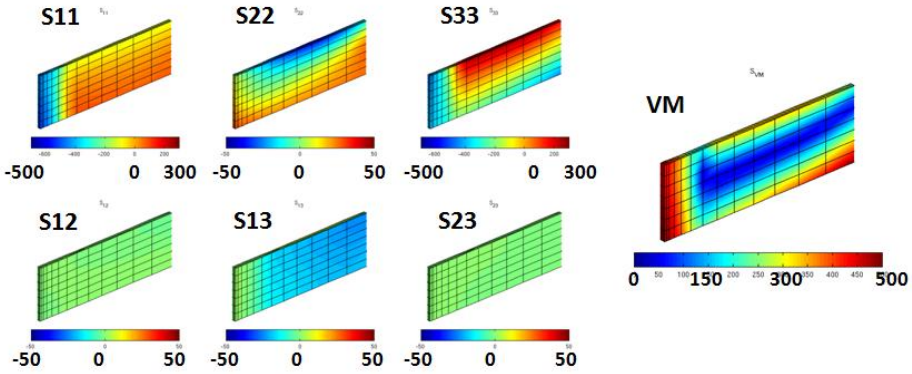

Figure 14: The components of the residual stress field obtained by the multiscale optimization method using the lattice strains shown in Figure 12. The second invariant of the residual stresses is also plotted.

peened sample can be obtained. Mimicking the volume of material interrogated by the x-rays, the finite element mesh of the sample is generated accordingly (Figure 13). Figure 14 shows the 3D residual stress distribution over the shot peened sample. The components of stresses that show the largest magnitudes are the 11- and the 33- components of stress while other components are closer to zero. Furthermore, as we expect from the lattice strain measurements, the stresses show a large gradient along y_S at the surface than in the interior. This is also visible in the plot of the second variant of the residual stress.

We also investigated the relationship between the quality of electron back scattered diffraction (EBSD) image and the residual stress field in the shot-peened sample. Figure 15 shows the region where the sample for the EBSD experiment was extracted from the original piece of the shot-peened material and the orientation map from the EBSD sample. The EBSD sample was extracted such that the it is from the mid-plane of the original piece of the shot-peened material in the z-direction. This means that on the EBSD map shown in Figure 15, the effects from the shot-peening process is concentrated at the top and at the bottom of the EBSD map the material is close to its virgin state.

Along with orientation information for each point on the EBSD sample, the mean angle deviation (MAD), band contrast (BC), and band slope (BS) data are available. These information can be used as an indicator of large deformation experienced by the material [6]. Using the EBSD data shown in Figure 15, averages of MAD, BC, and BS values are computed for each y-layer. The y-coorindate in this case is the distance from the shot-peened surface. Figure 16 shows the averages of MAD, BC, and BS values

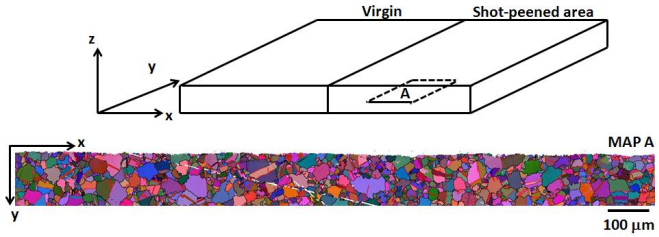

Figure 15: A schematic of the region where the sample for EBSD was extracted from the original piece of shot-peened material and the orientation map obtained from EBSD scan. Colors denote orientations.

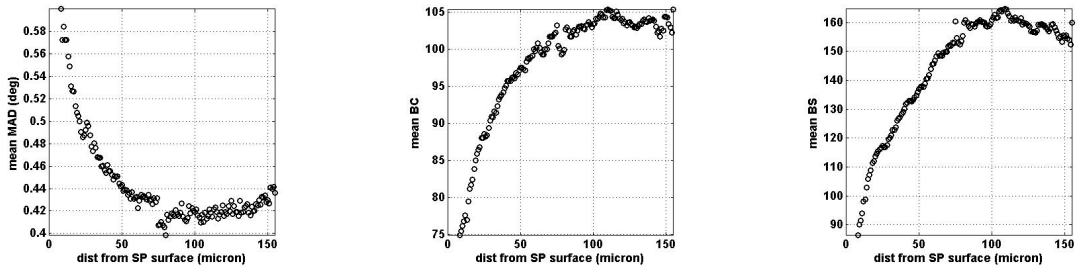

(a) The average mean angle deviation (MAD) per layer vs. distance from the surface plot.

(b) The average band contrast (BC) per layer vs. distance from the surface plot.

(c) The average band slope (BS) per layer vs. distance from the surface plot.

Figure 16: The results of the EBSD data.

plotted against the y-coordinate. The MAD value which indicates the angular deviation of the measured unit cell from the ideal unit cell should be smaller if the interrogated material experienced small plastic deformation. On the other hand, the BC and BS values are indicators of the Kikuchi pattern quality and they are larger if the interrogated material experienced small plastic deformation. Figure 16 shows that the MAD, BC, and BS values indicate a small layer (approximately 100 μm thick) with large plastic deformation. The layers located below 100 μm have nearly constant values of MAD, BC, and BS values. Comparing these plots with the effective stress shown in Figure 14, the layers of material with MAD, BS, and BC values that indicate large plastic deformation are where the effective stress is large.

While further investigation is necessary, these results show that the method that we have developed can be extended to real industrial applications.

7 Representation of orientation dependent crystal stresses

A component of orientation dependent crystal stress is represented by a set of orthonormal functions defined over orientation space and corresponding coefficients. This was described in Equation 4. Using this representation reduces the number of unknowns while enforcing a smooth variation of the orientation dependent stresses.

$$\sigma_{pq}(\boldsymbol{r}) = \sum_{m=1}^{m_{max}} H^m(\boldsymbol{r}) w_{pq}^m \tag{5}$$

For example, if the orientation space is discretized by 600 independent nodes, the total number of unknowns necessary for reprensenting the orientation dependent crystal stresses at a particular diffraction volume is 3,600. On the other hand, if the orientation dependent crystal stresses for a particular diffraction volume are represented by a set of orthonormal functions and corresponding coefficients, the total

number of unknowns necessary is $m_{max} \times 6$. This is quite beneficial when many diffraction volumes are interrogated.

While this is a large reduction of number of unknowns, we explored the idea of further reducing the number of unknowns by studying the relationhsip between the orientation dependent crystal stresses and the orthonormal functions. To investigate this relationship, crystal-based elastoplastic finite element simulations were performed using several instances of virtual polycrystals. From these simulations, it was determined that only a subset of the orthogonal functions are necessary to represent $\sigma_{pq}(\boldsymbol{r})$. This work has not been implemented in our residual stress methodology yet but will be beneficial as we start interrogating larger number of diffraction volumes in real engineering components.

8 Accomplishments and Future Directions

The project was extremely successful using several different metrics. At different times during the grant, 2 graduate students and 2 post-docs were supported. One masters thesis was completed with another anticipated in May, 2013. A paper describing the 2D method on the LSHR has appeared [2]. The paper describing the 3D experimental method [5] and the moving least squares method, [3], are in review. The paper on the titanium is in preparation [5] and one more is in preparation [7]. The shot-peened work may be written up for a paper but has certainly spawned a new White Paper written to the AFOSR proposing a combined diffraction / process simulation method for measuring residual stress [8]. In this work, we propose combining the biscale MLS method with reduced order simulations of shot peeing and laser shock peening processes to measure residual stress then to tune the processing parameters to optimize component performance.

References

[1] Ashish Kumar and P. R. Dawson. The simulation of texture evolution with finite elements over orientation space i. development. *Computer Methods in Applied Mechanics and Engineering*, 130(3-4):227–246, April 1996.

[2] K.P. McNelis, P.R. Dawson, and M.P. Miller. A two-scale methodology for determining the residual stresses in polycrystalline solids using high energy x-ray diffraction data. *Journal of Mechanics and Physics of Solids*, 61:428–449, 2013.

[3] Eralp Demir. Determination of depth-resolved residual stress using lattice strain pole figure measurements. *Computer Methods in Applied Mechanics and Engineering*, in review, 2013.

[4] Matthew Peter Miller, Joel Vincent Bernier, Jun-Sang Park, and Alexander Kazimirov. Experimental measurement of lattice strain pole figures using synchrotron x rays. *Review of Scientific Instruments*, 76:113903, 2005.

[5] Jun-Sang Park, Ulrich Lienert, Paul R. Dawson, and Matthew P. Miller. A non-destructive methodology for obtaining strain pole figures at internal points in a component using synchrotron radiation to determine its three dimensional residual stress field. *Experimental Mechanics*, submitted, 2012.

[6] A. J. Wilkinson and D. J. Dingley. Quantitative deformation studies using electron back scatter patterns. *Acta metall, mater.*, 39(12):3047, 1991.

[7] J-S. Park, A.K. Ray, U. Lienert, P. R. Dawson, J C Williams, and M. P. Miller. Determination of residual stress in a microtextured titanium using bi-scale optimization method. page In Preparation, 2013.

[8] M. P. Miller, A. J. Beaudoin, and J C Williams. A coordinated experimental/modeling methodology for evaluating residual stress fields in surface treated metals. White paper to afosr, Cornell University, 194 Rhodes Hall, Cornell University, Ithaca, NY, January 2013.